Conductance quantization in a periodically modulated channel

Manhua Leng and Craig S. Lent
Department of Electrical Engineering, University of Notre Dame, Notre Dame, Indiana 46556
(Received 30 June 1994)

The transport properties of a quantum channel with a periodically modulated conducting width are investigated. A single constriction has a quantized conductance and its conduction plateaus have finite rises. For a short channel with just a few periods of modulation, conductance is no longer quantized. For a long channel with many periods of modulation, the quantized conductance characteristic of a simple quantum point contact is recovered, but the index of the quantization plateaus is no longer a monotonically increasing function. Rather, the conductance steps up and down with energy. We calculate the energy band structure of the corresponding infinite modulated channel. Comparison between the quantized conductance and band structure shows a one-to-one correspondence between the plateau index and the number of Bloch bands with positive group velocity at a given energy. The nonmonotonic conductance quantization for a long channel persists in the presence of an applied magnetic field, as does the direct correspondence between the plateau index and the number of energy bands. In the high-field regime this can be interpreted as selective resonant backscattering of edge states, and lends to nonmonotonic plateaus in the Hall resistance in the integer quantum Hall effect.

I. INTRODUCTION

The first ballistic quantum point contact (QPC) devices were fabricated using a split-gate geometry patterned on top of a two-dimensional electron gas in high-mobility $GaAs/Al_xGa_{1-x}As$ semiconductor heterostructures by Wharam *et al.* and van Wees *et al.*[1,2] A negative voltage applied on the split gate depletes the electrons underneath the gate, creating a constriction for conduction between the two wide regions separated by the split gate. Only the open region between the two parts of the split gate allow the carriers to pass, forming a narrow conducting channel. At low temperatures, the conductance of such QPS's was found to decrease in a series of steps as the negative gate voltage was made more negative.

The physical origin of this quantization is understood to be (1) the creation of lateral one-dimensional subband modes, analogous to waveguide modes, due to the confinement by the constriction, and (2) the fact that each mode carries the same amount of current. In the linear-response regime, the conductance of the QPC can be described by employing the two-terminal Landauer conductance formula

$$G=(2e^2/h)\,\mathrm{Tr}(tt^{\dagger})=(2e^2/h)\sum_{i,j}|t_{i,j}|^2\ , \tag{1}$$

where t is the transmission amplitude matrix of the structure.[3] In the first model based on this formula, the t matrix was simply taken to be the transmission amplitudes of the narrow ballistic constriction, which has the property $|t_{i,j}|^2=\delta_{ij}$. Therefore the conductance is found to be $G(E)=(2e^2/h)N_t(E)$, where $N_t(E)$ is the number of traveling modes (subbands) in the constriction at energy E, a perfectly sharp integer step function.[2] The experimental results are in qualitative agreement with this argument, but not as sharp as implied.

As a result of the transverse modes produced by the lateral confinement, the conductance plateaus in a QPC increases monotonically in steps as additional traveling modes become available. If the ballistic channel is patterned with further features, bends, constrictions, other obstructions, or random potentials, conductance quantization is lost, and a complicated structure for $G(E)$ emerges due to the details of quantum interference and backscattering in the channel.[4–6]

However, if a ballistic channel has a periodically modulated structure, we find that the quantization in the conductance $G(E)$ is recovered: what is "lost" is the monotonic feature of $G(E)$ as a function of energy, as is the case in the conductance quantization of a QPC.[7,8] Instead, the index of conduction plateaus is a nonmonotonic integer function that steps up and down as energy increases.

In the presence of a perpendicular magnetic field, the conductance quantization of a QPC persists, as does the monotonic profile of its conduction plateaus.[9] Similarly, for a straight channel in the integer quantum Hall effect (IQHE) regime, Hall resistance plateaus step up monotonically in the well-known staircase fashion as magnetic field increases.[10] For a periodically modulated electron channel, our investigation shows that the conductance $G(B)=(2e^2/h)N(B)$ as a function of an applied magnetic field is also quantized, but the index of conduction plateaus $N(B)$ is a nonmonotonic integer function.

Our basic results concerning the recovery of the quantized conduction appeared in a recent paper.[7] In this paper we provide a fuller description of our calculation and extend the results of considering (1) the conduction as a function of applied magnetic field, (2) smooth variations in the channel walls, and (3) the connection to the integer quantum Hall effect.

The outline of this paper is as follows: Section II is a brief account of the theoretical model and numerical

method employed, Sec. III contains the calculated results and related discussion, and Sec. IV summarizes our results. In Appendix A, we outline the scattering-matrix cascading technique, which we utilize to obtain the transmission matrix of a periodic structure consisting of any number of unit cells. In Appendix B, we summarize our extension of the quantum transmitting-boundary method (QTBM), which we employ to solve the transport problem of open boundary conditions both in the absence and presence of a perpendicular magnetic field.

II. MODEL AND METHOD

The structure under investigation is shown schematically in Fig. 1. A channel of width W is periodically narrowed to a width of $w=W-h$ by an array of potential barriers ("fingers") on the upper edge of the channel. The period of the modulation is a, the number of narrow regions (the number of periods) is N, and the length of each narrow region in the longitudinal direction is d. We present results for the particular case where $W/a=2.0$, $h/a=0.6$, and $d/a=0.4$. A magnetic field of magnitude B is applied in the $\hat{z}$ direction, perpendicular to the xy plane where the conducting channel is. The Landau gauge is chosen for the vector potential so $\vec{A}=-By\hat{x}$. We adopt a single-band effective-mass model with an effective mass $m^*/m_0=0.067$, appropriate for GaAs. Spin is accounted for through the twofold degeneracy in the Landauer formula and is ignored otherwise throughout the calculation. Hard-wall potentials are assumed to define the channel modulation while the potential inside the channel is taken to be zero.

We solve the two-dimensional time-independent Schrödinger equation

$$\left[\frac{-\hbar^2}{2m^*}\nabla^2+\frac{i|e|\hbar By}{m^*}\frac{\partial}{\partial x}+\frac{|e|^2B^2y^2}{2m^*}+V_0(x,y)\right]\Psi(x,y)=E\Psi(x,y)\ . \quad (2)$$

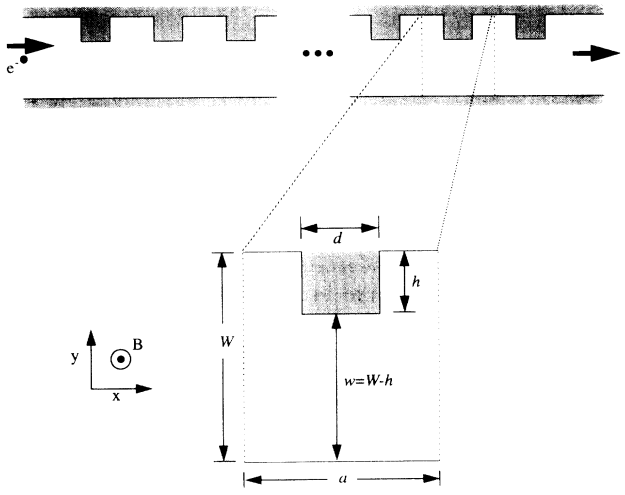

FIG. 1. The geometry of the periodically modulated quantum channel.

To calculate the conductance of a channel of finite length with N periods, we solve Eq. (2) to obtain the complex energy-dependent transmission and reflection amplitudes for each transverse mode, defined in the wide regions. We solve directly for the wave function and transmission amplitudes in one unit cell (marked by dashed lines in Fig. 1), then use a scattering-matrix cascading method[11] to obtain transmission and reflection amplitudes for the whole structure consisting of N unit cells. Transmission and reflection into evanescent modes must be included in the cascading process (see Appendix A for the details of the scattering-matrix cascading). The conductance in the linear response regime is then obtained using the two-terminal version of the Landauer formula.[3,12]

The numerical solution of Eq. (2) for the unit cell with open boundary conditions is accomplished using the quantum transmitting-boundary method,[13] a numerical algorithm we have developed based on the finite-element method for solving the two-dimensional Schrödinger equation for current-carrying states. We employ a recent extension of the method to include the effects of an applied magnetic field.[14] A synopsis of the quantum transmitting-boundary method in a magnetic field is provided in Appendix B. Transmission is computed at fixed magnetic field on a very fine energy mesh. Transmission as a function of magnetic field at fixed incident energy is also computed. Real-space discretization requires meshes of 50×100 elements at high values of magnetic field.

We compare the conductance for the finite system with N periods of modulation with the energy band structure of the corresponding infinite periodic system. For the infinite system, we use the Bloch theorem and look for a solution of the form $\Psi_{n,k}(x,y)=e^{ikx}u_{n,k}(x,y)$, where $u_{n,k}(x,y)$ is the periodic part of the Bloch wave function and k is the wave vector. With this substitution, the resulting Schrödinger equation as an eigenvalue problem for $E_n(k)$ and $u_{n,k}(x,y)$ can be written as

$$\left[\frac{-\hbar^2}{2m^*}\nabla^2-\frac{i\hbar^2}{m^*}\left[k-\frac{|e|By}{\hbar}\right]\frac{\partial}{\partial x}+\frac{\hbar^2}{2m^*}\left[k-\frac{|e|By}{\hbar}\right]^2+V\right]u_{n,k}(x,y)=E_n(k)u_{n,k}(x,y)\ . \quad (3)$$

We use the finite-element method to achieve numerical discretization over the unit cell. A subspace iteration technique is used to obtain the lowest several eigenenergies for several values of wave vector k spanning the first Brillouin zone. Meshes of up to 5151 nodes were used to achieve convergence at high values of magnetic field.

III. RESULTS AND DISCUSSIONS

A. Conductance quantization at zero magnetic field

Figure 2 shows the calculated conductance for finite channels and the band structure for an infinite channel when no magnetic field is applied ($\beta=0$). Energy is expressed in units of E_1, the energy of the first transverse mode (subband) in the wide regions defined as

$$E_1=\frac{\hbar^2}{2m^*}\left[\frac{\pi}{W}\right]^2. \tag{4}$$

The horizontal axis is plotted as $\sqrt{E/E_1}$, for simple comparison between the rising location of the conductance for a short channel and the turn-on energies of the successive modes (at $\sqrt{E/E_1}=1,2,3,\ldots$), which are defined in the *wide* regions. Figures 2(a), 2(b), 2(c), and 2(e) show the conductance of a channel with $N=1$, 2, 16, and 85 unit cells (constrictions), respectively. The energy band structure for the infinite modulated channel is shown for the first Brillouin zone in Fig. 2(f). Energy is plotted on the horizontal axis so that the relationship to the conductance results below is clear. Figure 2(d) shows the individual transmission coefficients for each incident mode ($T_1, T_2, \ldots$), defined in the wide region, for the long channel with $N=85$ periods. The vertical scale is for the transmission coefficient of the first mode, T_1. For clarity, curves T_2, T_3, T_4, and T_5 are offset by 1.0, 2.0, 3.0, and 4.0, respectively.

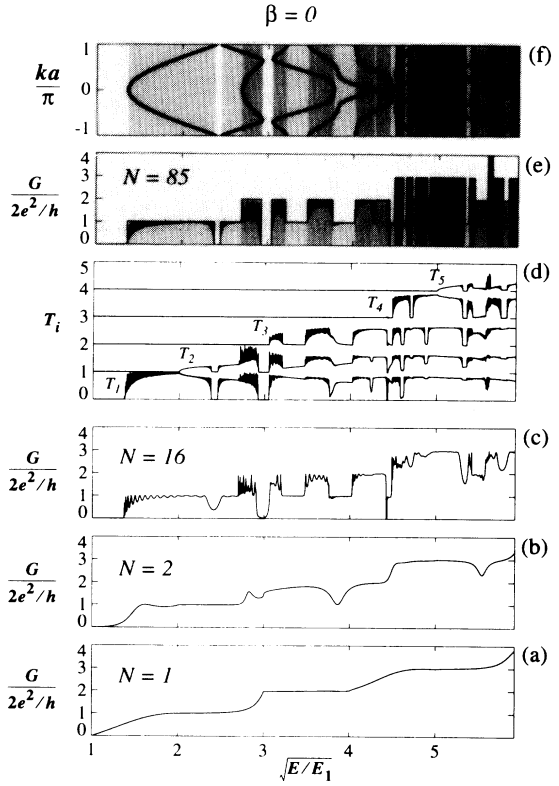

FIG. 2. The modulated channel in no applied magnetic field. (a) Conductance for a short channel with 1 unit cell ($N=1$): a QPC structure. (b) Conductance for a short channel with 2 unit cells ($N=2$). (c) Conductance for a channel with 16 unit cells ($N=16$). (d) Transmission coefficients of individual modes for a long channel with 85 unit cells ($N=85$). (e) Conductance for the long channel with $N=85$ unit cells. Gray-scale shadings indicate the index of the quantization plateau. (f) The energy band structure for the infinite periodic channel. Gray-scale shadings indicate the number of individual energy bands with positive group velocity in each energy region. The correspondence of the shading schemes in (e) and (f) illustrates that the conductance of the finite channel is related to the number of positive-velocity bands in the band structure of the infinite channel.

For a single constriction ($N=1$) in the channel which forms a QPC, the conductance, plotted in Fig. 2(a), shows an overall quantization profile, which increases monotonically with energy. The conductance plateaus start to rise at the turn-on energies of the traveling modes in the *wide* region, which is lower than the turn-on energies of the traveling modes in the constriction by a factor of $(W/w)^2$ (2.04 in our case). The rise is gradual, "inherent" to the QPC conductance because of the mismatch between the electron states in the wide region and narrow regions.[15–17] This is enhanced by the contribution from the evanescent modes because the constriction is short in our case where $d/w=\frac{2}{7}$. For two constrictions ($N=2$) in the channel, the conductance, plotted in Fig. 2(b), is not quantized and shows more structures. This is to be expected because of details of mode mixing due to the abrupt narrowing of the channel and the resonant state formed between the two constrictions.[18]

For a channel with $N=16$ constrictions, the conductance, plotted in Fig. 2(c), shows a clear profile of quantization. There is also an indication of the familiar miniband formation in a periodic structure.[19] Although the basic features of the quantization are already present for channels with comparatively few periods, such as the one just shown in Fig. 2(c), some narrow and fine plateaus reveal themselves only for a rather long channel, as shown in Fig. 2(e) for a channel with $N=85$ periods. Figure 2(f) shows that for no individual incident mode of the long modulated channel ($N=85$) is the transmission quantized. However, the total conductance, which is the sum of the modal transmissions as shown in Fig. 2(d), is striking in that it is essentially quantized in units of $2e^2/h$. Unlike the usual quantization of QPC ballistic conductance, however, the conductance of the modulated long channel does not increase monotonically but rather steps up *and down* between quantized levels, sometimes going to zero.[20] We write the ballistic conductance of the very long channel as $G(E)=(2e^2/h)N_c(E)$, where $N_c(E)$ is the integer index corresponding to the quantized conductance plateau for energy E, a nonmonotonic piecewise constant function of energy.

The rapid oscillations seen in Figs. 2(c) and 2(e) originate from the coupling of the quasi-zero-dimensional states in the cavities formed between narrow regions. These are closely related to transmission poles in the complex energy plane off the real axis.[21,22] In the first conduction plateau the number of oscillations is equal to the number of cavity regions ($N-1$). These are well resolved in our current energy mesh for $N=16$ in Fig. 2(c), but not so well resolved for $N=85$ in Fig. 2(e). At higher energies, the oscillations are complicated by mode mixing when more than one transverse subband in the narrow regions exists. So the number of oscillations has no simple direct correspondence to the number of quasi-one-dimensional states (equivalently the number of cavity regions). Note that for some plateaus the oscillations are absent and the conductance for these plateaus converge

to the exact quantized values more quickly while for some other plateaus the oscillations persist. We suggest that this has to do with the inherent incommensurability in the corrugated structure, a full discussion of which will be given elsewhere.[22]

The conductance quantization in Fig. 2(e) can be understood by examining the band structure shown in Fig. 2(f). For each value of the energy, define an integer $N_b^+(E)$ to be the number of energy bands [distinct $E_n(k)$ curves] with positive group velocity (slope), $\vec{v}_g = \partial E(k)/\partial \vec{k} > 0$. From Fig. 2(e) we find that $N_b^+(E)$ is also a nonmonotonic function; it is zero in energy gaps and steps up and down as a function of energy. By comparing Figs. 2(e) and 2(f) we see that, in fact, $N_c(E) = N_b^+(E)$. The number of positive velocity bands for the infinite system yields the quantization of the conductance in the periodically modulated finite system. The shaded regions of the figures illustrate this correspondence with each value of $N_c(E) = N_b^+(E)$ represented by a different gray-scale value.

In a straight quantum waveguide, the conducting channels are the transverse subbands produced by a lateral confinement potential. The number of these modes, $N_b^+(E)$, is a monotonic increasing function of energy. The cancellation of the velocity and density of states leads to an identical current being carried by each subband. At higher energies, more of these ballistic channels are opened for conduction, so conductance goes up in a staircase fashion accordingly.

In the limit of many unit cells ($N \to \infty$) of periodically modulated channel, Bloch states are the counterparts of the transverse modes of the straight-through electron waveguide and they serve as the ballistic channels for transmission of electrons in the periodic structure. Like a strict one-dimensional periodic potential, the cancellation of velocity and density of states persists in the Bloch bands of a quasi-one-dimensional periodic channel. But in a strict one-dimensional (1D) periodic structure, $N_b^+(E)$ only takes the values of 1 in a band or 0 in a gap. In the periodically modulated quasi-2D channel, however, $N_b^+(E)$ can take other integer values as well. This behavior of $N_b^+(E)$ is a result of the interplay between the longitudinal periodicity and the transverse confinement potential. In the limit of infinite periodic structure, Bragg reflections and mode mixing result in the appearance of forbidden gaps and allowed energy regions with differing numbers of energy bands. In finite but long structure, the mode mixing and reflection result in nonmonotonic conductance quantization. In terms of transverse modes produced solely by the lateral confinement, transport is by no means adiabatic; however, transport can be viewed as the adiabatic transmission of Bloch states.

It is important to note that the transmission of individual modes is *not quantized,* but the total transmission is. The quantization occurs as the various modes are mixed by the periodic scattering. The nonmonotonic conductance quantization for the modulated channel is therefore a manifestation of the two-dimensional character of the channel mixing and the quasi-one-dimensional character of the current flow.

B. Conductance quantization in a magnetic field

In zero magnetic field, the electrostatic confinement potential across the channel in the $\hat{y}$ direction gives rise to the transverse modes (subbands). In high magnetic fields, the subbands are the magnetic edge states, which move in opposite directions along the opposite channel walls. Following Büttiker's interpretation, we understand that in the limit of high magnetic fields, all transport would be through edge states and the suppression of backscattering between edge states on opposite sides of the channel would guarantee monotonically increasing and quantized conductance.[23] In the field range of intermediate strength, however, both the electrostatic confining potential and magnetic field are important, giving rise to magnetoelectric subbands.[9,24] Mixing between the subbands can still occur and backscattering of edge states can still take place, producing rich structure in electromagneto transport. We now study the modulated channel in this field range. The magnetic field of magnitude B is described by a dimensionless parameter β, defined as

$$\beta \equiv \left[\frac{eB}{\hbar}\right] aW \equiv \frac{aW}{l_H^2} , \tag{5}$$

where $l_H = \sqrt{\hbar/eB}$ is the magnetic length. Energy is naturally expressed in units of the first bulk Landau level $E_L = \hbar\omega_c/2 \equiv \hbar(eB/2m^*)$.

In Fig. 3 we show the conductance and band structure calculated for the case of a magnetic field $\beta = 10$. For a single short constriction ($N = 1$), the conductance, plotted in Fig. 3(a), shows monotonically increasing steps with finite rise. For a channel with $N = 3$ periods, the conductance, plotted in Fig. 3(b), shows some detailed structures and the quantization is "lost" due to the mode mixing in the channel. For a channel with $N = 16$ periods, however, the conductance quantization evidently emerges as shown in Fig. 3(c). For a long channel with $N = 60$ periods, the conductance, plotted in Fig. 3(e), is more prominently quantized. The individual modal transmission coefficients for $N = 60$ are plotted in Fig. 3(d). As in zero magnetic field, none of them shows quantization by themselves. It is only the total transmission coefficient (equivalently conductance), which is a sum over all the modal transmission coefficients, that is quantized. Again, this quantization is nonmonotonic and related directly to the number of positive-velocity bands in the band structure for the corresponding infinite system, shown in Fig. 3(f).[25] So, if we write the conductance of the very long channel as a function of energy at a fixed magnetic field as $G(E)|_B = (2e^2/h)N_c(E)|_B$, where $N_c(E)|_B$ is the integer index of the conduction plateau, we will have $N_c(E)|_B = N_b^+(E)|_B$, where $N_b^+(E)|_B$ is the number of Bloch bands with positive group velocity in the energy band structure.

For the results shown in Fig. 3, the corrugations are only in the interior region between the contacts but the long lead regions, which connect the corrugated region to the contacts, are considered straight. A two-terminal measurement configuration for such a channel is illustrat-

ed in Fig. 4(a). Electrons are injected from the source onto the transverse modes defined in the straight leads. Upon entering the corrugated region, the incident waves are scattered by the corrugations, resulting in a certain amount of reflection. For a channel with $N=60$ periods at a magnetic field of $\beta=20$, the calculated conductance is plotted in Fig. 4(b). It shows the characteristic of the nonmonotonic quantization steps.

In Fig. 4(c), we plot the modal transmission coefficients for the individual incident edge states. Note in Fig. 4(b) that the conductance is lowered by one unit for energies just below $7E_L$, marked by the dashed line. Examination of the individual transmission coefficients in Fig. 4(c) shows that it is the *first* edge state (with a slight admixture of the third) that has been resonantly reflected. For this energy range the second and third edge states are almost entirely transmitted but the first and outermost

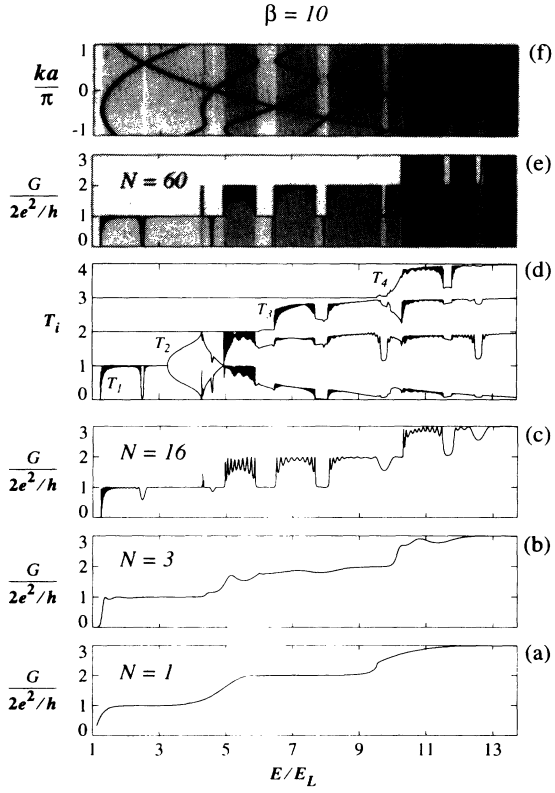

FIG. 3. The modulated channel in an applied magnetic field of $\beta=10$. (a) Conductance for a short channel with 1 unit cell ($N=1$): a QPC structure. (b) Conductance for a short channel with 2 unit cells ($N=3$). (c) Conductance for a channel with 16 unit cells ($N=16$). (d) Transmission coefficients of individual modes (edge states) for a long channel with 60 unit cells ($N=60$). (e) Conductance for the long channel with $N=60$ unit cells. Gray-scale shadings indicate the index of the quantization plateau. (f) The energy band structure for the infinite periodic channel. Gray-scale shadings indicate the number of individual energy bands with positive group velocity in each energy region. The correspondence of the shading schemes in (e) and (f) illustrates that the conductance of the finite channel is related to the number of positive-velocity bands in the band structure of the infinite channel.

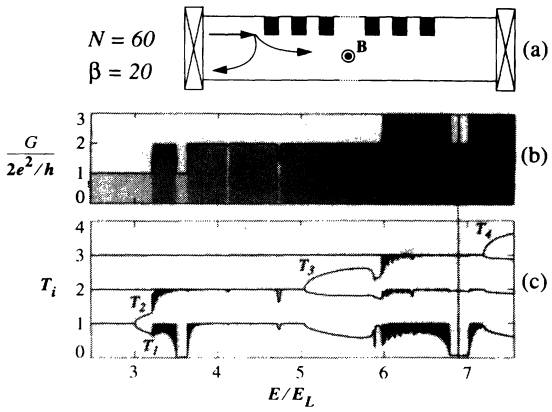

FIG. 4. (a) A modulated channel with straight leads connected to the source and drain. Incident electrons are in the subbands defined in the straight lead regions. (b) Conductance for such a channel with $N=60$ unit cells. (c) Transmission coefficients of individual modes (edge states).

edge states is reflected.

Figure 5 is a configuration of Hall resistance and two-terminal resistance measurements. Under the assumption of local equilibrium, the channel upper edge is at equipotential with the current source $E_f+\delta\mu$ and the channel lower edge at equipotential with the current drain E_f. The two-terminal resistance is $R_{2t}=V_{13}/I_{13}=\delta\mu/I_{13}$ and the Hall resistance is $R_H=V_{24}/I_{13}=\delta\mu/I_{13}$. Thus, they are equal to each other in this case.[26]

Suppose we consider a very long channel ($N\to\infty$) with the periodic corrugation extending to the lead (contact) regions as schematically shown in Fig. 6(a). Assume the incident electrons are injected by the contacts in Bloch states. Since Bloch states themselves are the results of the reflection due to the periodic corrugations, there will be no further internal or mode mixing for such incident electrons and hence no backscattering. This is similar to the phenomenon of the suppression of backscattering of edge states in the integer quantum Hall effect regime. Measurement of the two-terminal conductance for such a channel yields equivalently the inverse of the Hall resistance. In Fig. 6(b) we plot the energy band

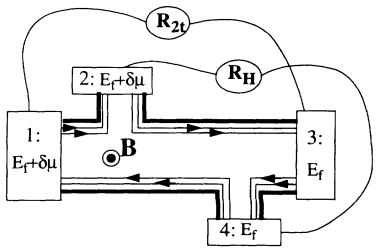

FIG. 5. A measurement configuration of two-terminal and Hall resistance. Under the conditions of local equilibrium, the channel upper edge is in equipotential with the current source and the lower edge is in equipotential with the current drain. The two-terminal resistance is equal to the Hall resistance.

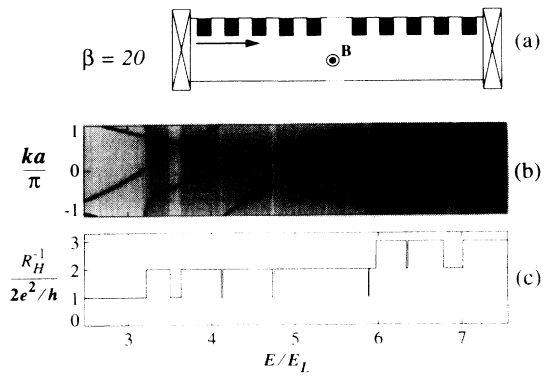

FIG. 6. (a) A very long modulated channel with modulations extended to the leads. Electrons are injected from the source onto the Bloch states. No backscattering occurs for such incident electrons. The two-terminal conductance is equivalent to the inverse of the Hall resistance. (b) The energy-band structure for the infinite periodic channel at $\beta=20$. (c) The inverse of the Hall resistance derived from the energy band structure.

structure for an infinite channel at $\beta=20$. From the correspondence between the conductance quantization for a very long channel and the band structure for the corresponding infinite periodic systems we observed and discussed above, we can derive the Hall conductance for such structure as $R_H^{-1}=(2e^2/h)N_c=(2e^2/h)N_b^+$. This is plotted in Fig. 6(c). Therefore, the simple, nonmonotonic feature of the energy band structure yields the exact, nonmonotonic quantization of the Hall resistance. Here we plot R_H^{-1} as a function of the Fermi energy, compatible with the original IQHE experimental results of von Klitzing, Dorda, and Pepper, where the Hall resistance was investigated as a function of gate voltage.[27]

C. Conductance quantization as a function of magnetic field

To complete our investigation of magnetotransport, we present in Fig. 7 the calculated transmission and conductance results versus the applied magnetic field at a fixed energy of $E=30E_1$, where E_1 is the energy of the first subband when no magnetic field is present as defined in Sec. III A. There exist five traveling modes at zero magnetic field. The strength of the magnetic field is measured by the parameter β, as defined in Eq. (5).

Figures 7(a), 7(b), and 7(c) plot the conductance of a channel with $N=4$, 50, and 250 periods, respectively. The short channel with $N=4$ modulations shows no quantization; the long channel with $N=50$ modulations shows strong signal of quantization; the *very* long channel with $N=250$ modulations shows clear quantized steps. As the conductance plateaus step up and down in the increasing magnetic field, the quantization manifests its nonmonotonic characteristic. Once again, the individual transmissions of even the very long channel, plotted in Fig. 7(d), have complicated features as a function of magnetic field.

In a simple ballistic QPC, the index of the conductance plateau is a decreasing staircase function as an increasing

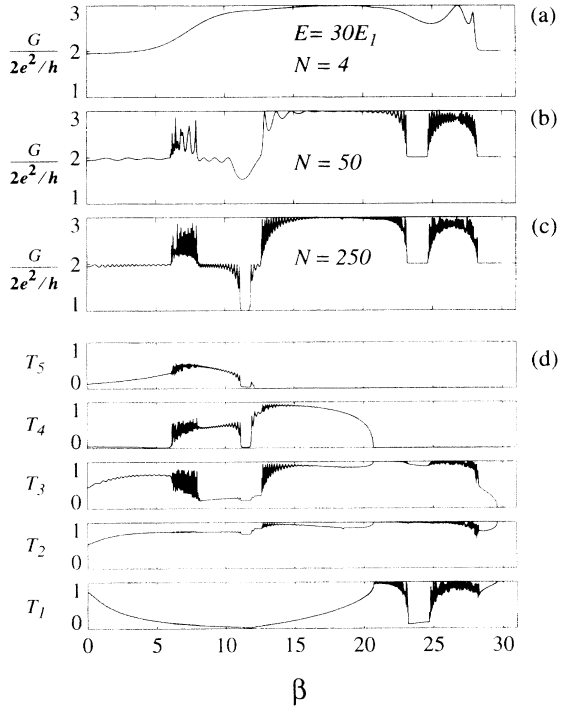

FIG. 7. The modulated channel in a varying magnetic field at an energy of $E=30E_1$. (a) Conductance for a short channel with 4 unit cells ($N=4$). (b) Conductance for a long channel with 50 unit cells ($N=50$). (c) Conductance for a very long channel with 250 unit cells ($N=250$). (d) Transmission coefficients of individual modes (edge states) for the long modulated channel.

magnetic field depopulates successive magnetoelectrostatic energy subbands below the Fermi energy. In a straight waveguide, Hall conductance (or resistance) in the integer quantum Hall effect regime has similar monotonic behavior in a varying magnetic field. However, in the periodically corrugated ballistic channel under discussion, the conductance, written as $G(B)=(2e^2/h)N_c(B)$, is quantized in a nonmonotonic fashion, with $N_c(B)$ being the integer index of the conductance quantization plateau at magnetic field B. In the case of varying magnetic field, there exists no single energy-band diagram for the corresponding infinite structure. An argument can be made in terms of an instantaneous energy-band structure for each field value. The conclusion of $N_c(E)=N_b^+(E)$, drawn in Sec. III A, then can be extended to $N_c(E,B)=N_b^+(E,B)$. Here $N_b^+(E,B)$ is the number of positive-velocity Bloch states for the corresponding infinite structure at a given set of energy E and magnetic field B.

We have mentioned the resonance reflection of the first edge state in Figs. 4(d) and 4(e) over a range of energy just below $7E_L$ at $\beta=20$. This is also observed in Fig. 7(d) over a range of magnetic field just below $\beta=25$ at $E=30E_1$. This selective reflection of edge states is similar to the experimental results of Müller *et al.*,[28] where they used an applied potential from a metal gate to reflect individual edge states. The consequence of this reflection was a deviation from the usual integer quantum Hall

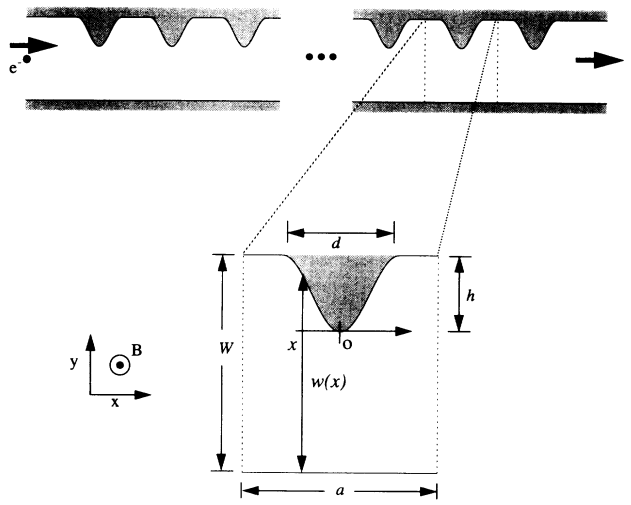

FIG. 8. The geometry of a periodically modulated quantum channel with sinusoidal modulations.

effect (IQHE) plateaus, a deviation understandable in the edge-state picture of the IQHE.[23] The reflection of selective edge states seen in our calculation for a modulated channel suggests that a similar IQHE deviation, steps up and down between Hall resistance plateaus, should be observable in these geometries.

D. A sinusoidally corrugated channel

To show that the recovery of the conductance quantization is not an artificial effect due to the abrupt, sharp nature of the corrugations, we consider a quantum channel with a smoothly varying width. Figure 8 schematically shows this geometry. The upper wall of the channel is periodically modulated by a sinusoidal corrugation. The corrugation has a maximum width h extended into the channel and a maximum extension d in the longitudinal direction. The conducting width of the channel

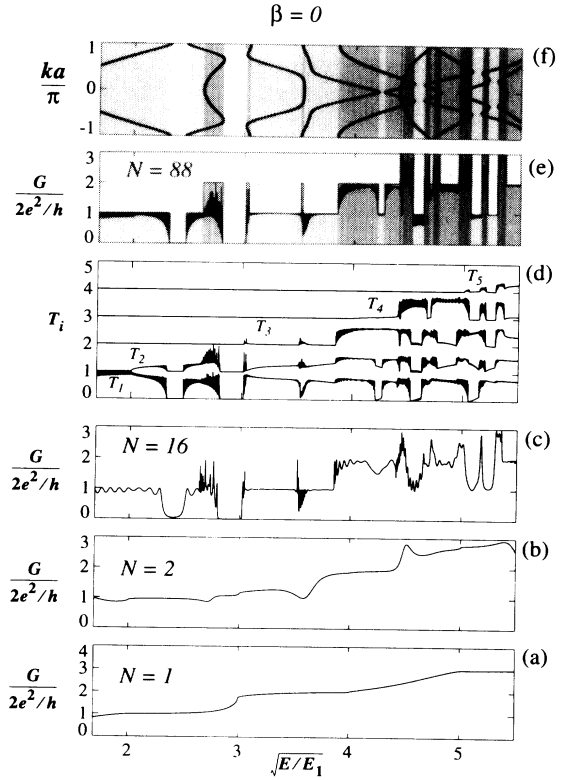

FIG. 9. The sinusoidally modulated channel in no applied magnetic field. (a) Conductance for a short channel with 1 unit cell ($N=1$): a QPC structure. (b) Conductance for a short channel with 2 unit cells ($N=2$). (c) Conductance for a channel with 16 unit cells ($N=16$). (d) Transmission coefficients of individual modes for a long channel with 88 unit cells ($N=88$). (e) Conductance for the long channel with $N=88$ unit cells. Gray-scale shadings indicate the index of the quantization plateau. (f) The energy band structure for the infinite periodic channel. Gray-scale shadings indicate the number of individual energy bands with positive group velocity in each energy region. The correspondence of the shading schemes in (e) and (f) illustrates that the conductance of the finite channel is related to the number of positive-velocity bands in the band structure of the infinite channel.

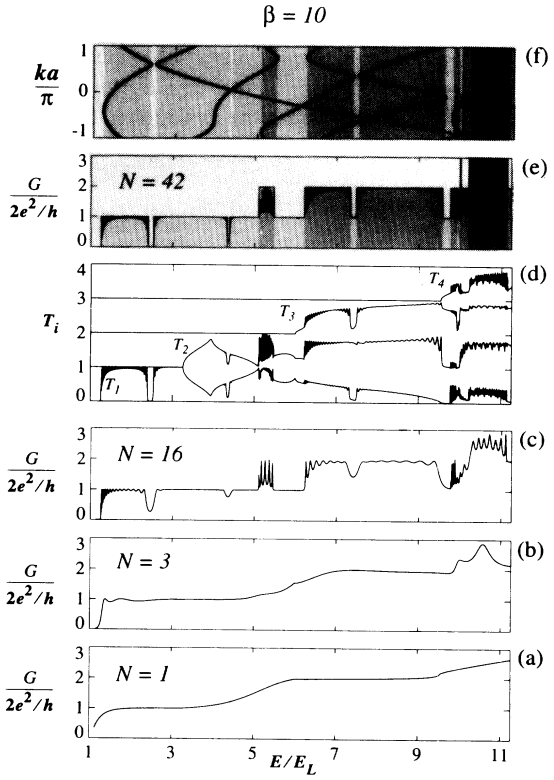

FIG. 10. The sinusoidally modulated channel in an applied magnetic field of $\beta=10$. (a) Conductance for a short channel with 1 unit cell ($N=1$): a QPC structure. (b) Conductance for a short channel with 2 unit cells ($N=3$). (c) Conductance for a channel with 16 unit cells ($N=16$). (d) Transmission coefficients of individual modes (edge states) for a long channel with 42 unit cells ($N=42$). (e) Conductance for the long channel with $N=42$ unit cells. Gray-scale shadings indicate the index of the quantization plateau. (f) The energy band structure for the infinite periodic channel. Gray-scale shadings indicate the number of individual energy bands with positive group velocity in each energy region. The correspondence of the shading schemes in (e) and (f) illustrates that the conductance of the finite channel is related to the number of positive-velocity bands in the band structure of the infinite channel.

$w(x)=W-h(\cos\pi x/d)^2$ varies between W and $W-h$ continuously and its first derivative is also continuous. The calculated conductance and band structure are plotted for the case of $W/a=2.0$, $h/a=0.7$ and $d/a=0.6$ at zero magnetic field in Fig. 9 and at a magnetic field of $\beta=10$ in Fig. 10.

Similar examinations of the conductance (transmission) for short channels and long channels are conducted as we have discussed in previous sections for the abruptly corrugated structure. The conductance quantization of a single ballistic constriction ($N=1$) as shown in Figs. 9(a) and 10(a) has a finite rise in plateaus. This quantization is lost in a short channel with just a few modulations as shown in Figs. 9(b) and 10(b) for $N=3$. For long structures with many periodic modulations, however, the conductance quantization is recovered and is characteristically nonmonotonic, with and without magnetic fields as shown in Figs. 9(e) and 10(e). Comparison with the energy band structure maintains the conclusion of $N_c(E,B)=N_b^+(E,B)$, where $N_c(E,B)$ is the index of the conductance plateau for the long but finite periodic channel and $N_b^+(E,B)$ is the number of positive-velocity Bloch states (energy bands) for the corresponding infinite structure. We conclude that the nonmonotonic conductance quantization we have discussed so far is indeed due to the periodic nature of the structure and not an artifact of the abruptness of the corrugations.

IV. CONCLUSION

In conclusion, we have studied the ballistic transport properties of periodically modulated channels. In a single short constriction, the well-known conductance quantization of a QPC is present, but the plateaus rise gradually due to the impedance mismatch and effects of evanescent states. This quantization is destroyed for short channels with a few periodic constrictions. For a long modulated channel, however, our result show that ballistic conductance is again quantized, but is a nonmonotonic function of energy. The index of a quantized conductance plateau has a one-to-one correspondence to the number of positive-velocity states in the energy band structure for the corresponding infinite modulated channel. Like the one-dimensional subbands in a QPC, each Bloch state in a periodic quasi-one-dimensional structure carries the same amount of current; this gives the physical origin of the conductance quantization observed in our calculations. Unlike the counterpart 1D subbands in straight channels, the number of Bloch states in a periodic channel is not a monotonic function of energy; this accounts for the nonmonotonic behavior of the conductance plateaus. This phenomenon persists in a varying magnetic field. At high magnetic field, it can be interpreted as a resonant reflection of particular edge states and should produce anomalous IQHE behavior.

An experimental investigation of the conductance of a modulated channel (16 periods) of the type shown in Fig. 1 has been performed,[19] but their results are for the energy region *below* the second conductance plateau and so probe only the purely one-dimensional aspect of this problem. Our findings of the nonmonotonic conductance quantization are the result of the quasi-two-dimensionality of the subbands, regardless of their electric or magnetic origin, and the mode mixing due to the scattering by the periodicity of the system. The experiments in Ref. 19 do illustrate that it is possible to observe the effects of coherence over many periods (and several micrometers).

ACKNOWLEDGMENTS

This work was supported by the Air Force Office of Science Research. The authors wold like to thank Dr. W. Porod and Z. Shao for helpful discussions.

APPENDIX A: SCATTERING-MATRIX CASCADING METHOD

The scattering matrix of a device describes the relationship between the outgoing current amplitudes and the incoming current amplitudes at its two ends. For a two-dimensional device in which transverse modes arise due to a confining potential, the scattering matrix relates the amplitudes of the wave function projected onto the outgoing modes and the amplitudes of the wave function projected onto the incoming modes. Shown in Fig. 11 is a device consisting of two successive sections that are described by scattering matrices s_1 and s_2, respectively,

$$\begin{bmatrix} J^1_{\text{out}} \\ J_+ \end{bmatrix} = s_1 \begin{bmatrix} J^1_{\text{in}} \\ J_- \end{bmatrix} = \begin{bmatrix} r_1 & t'_1 \\ t_1 & r'_1 \end{bmatrix} \begin{bmatrix} J^1_{\text{in}} \\ J_- \end{bmatrix}, \tag{A1}$$

$$\begin{bmatrix} J_- \\ J^2_{\text{out}} \end{bmatrix} = s_2 \begin{bmatrix} J_+ \\ J^2_{\text{in}} \end{bmatrix} = \begin{bmatrix} r_2 & t'_2 \\ t_2 & r'_2 \end{bmatrix} \begin{bmatrix} J_+ \\ J^2_{\text{in}} \end{bmatrix}, \tag{A2}$$

where $\{J^1_{\text{in}}\}$ and $\{J^1_{\text{out}}\}$ are the amplitudes of the incoming and outgoing states at interface 1; $\{J^2_{\text{in}}\}$ and $\{J^2_{\text{out}}\}$ are the amplitudes of the incoming and outgoing states at interface 2; $\{J_+\}$ and $\{J_-\}$ are the amplitudes of the right-going and left-going states at the internal interface II of the two sections. The dimensions of the above-defined $\{J\}$ vectors and the complex reflection and transmission matrices of s_1 and s_2 are

$$\{J^1_{\text{in}}\}:\ N^1_{\text{in}}\times 1\ ,\quad \{J^1_{\text{out}}\}:\ N^1_{\text{out}}\times 1\ , \tag{A3}$$

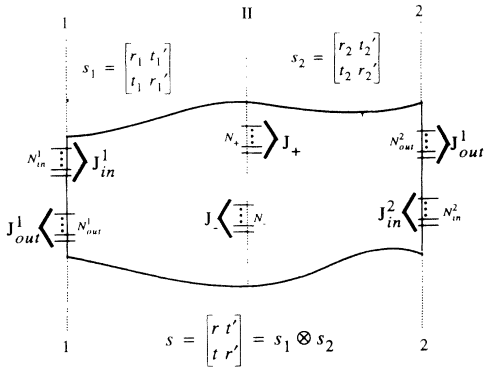

FIG. 11. A schematic diagram for scattering-matrix cascading.

$$\{J^2_{\text{in}}\}:\ N^2_{\text{in}}\times 1\ ,\quad \{J^2_{\text{out}}\}:\ N^2_{\text{out}}\times 1\ , \tag{A4}$$

$$\{J_+\}:\ N_+\times 1\ ,\quad \{J_-\}:\ N_-\times 1\ , \tag{A5}$$

$$r_1:\ N^1_{\text{out}}\times N^1_{\text{in}}\ ,\quad t_1: N_+\times N^1_{\text{in}}\ , \tag{A6}$$

$$r'_1:\ N_+\times N_-\ ,\quad t'_1: N^1_{\text{out}}\times N_-\ , \tag{A7}$$

$$r_2:\ N_-\times N_+\ ,\quad t_2:\ N^2_{\text{out}}\times N_+\ , \tag{A8}$$

$$r'_1:\ N^2_{\text{out}}\times N^2_{\text{in}}\ ,\quad t'_1:\ N_-\times N^2_{\text{in}}\ , \tag{A9}$$

where N^1_{in} is the number of incoming modes and N^1_{out} is the number of outgoing modes at interface 1; N^2_{in} is the number of incoming states and N^2_{out} is the number of outgoing states at interface 2; N_+ is the number of right-going modes and N_- is the number of left-going modes at the internal interface II.

Matrix equations (A1) and (A2) can be written as

$$J^1_{\text{out}}=r_1J^1_{\text{in}}+t'_1J_-\ , \tag{A10}$$

$$J_+=t_1J^1_{\text{in}}+r'_1J_-\ , \tag{A11}$$

$$J_-=r_2J_++t'_2J^2_{\text{in}}\ , \tag{A12}$$

$$J^2_{\text{out}}=t_2J_++r'_2J^2_{\text{in}}\ . \tag{A13}$$

By substituting Eq. (A12) into Eq. (A16), we get the following expression for J_+:

$$J_+=(I_+-r'_1r_2)^{-1}t_1J^1_{\text{in}}+(I_+-r'_1r_2)^{-1}r'_1t'_2J^2_{\text{in}}\ , \tag{A14}$$

where I_+ is an identity matrix of dimension $N_+\times N_+$. Then substitute Eq. (A14) into Eq. (A12); we get

$$J_-=r_2(I_+-r'_1r_2)^{-1}t_1J^1_{\text{in}} +[r_2(I_+-r'_1r_2)^{-1}r'_1t'_2+t'_2]J^2_{\text{in}}\ . \tag{A15}$$

With J^- and J^+ replaced by Eqs. (A14) and (A15), Eqs. (A10) and (A13) become

$$J^1_{\text{out}}=[r_1+t'_1r_2(I_+-r'_1r_2)^{-1}t_1]J^1_{\text{in}} +t'_1[r_2(I_+-r'_1r_2)^{-1}r'_1t'_2+t'_2]J^2_{\text{in}}\ , \tag{A16}$$

$$J^2_{\text{out}}=[t_2(I_+-r'_1r_2)^{-1}t_1]J^1_{\text{in}} +[t_2(I_+-r'_1r_2)^{-1}r'_1t'_2+r'_2]J^2_{\text{in}}\ . \tag{A17}$$

Let the overall scattering matrix of the whole device be s. Then the outgoing waves $\{J^1_{\text{out}}\}$ and $\{J^2_{\text{out}}\}$ are related to the incoming waves $\{J^1_{\text{in}}\}$ and $\{J^2_{\text{in}}\}$ through the total reflection and transmission matrices by the following matrix equation:

$$\begin{bmatrix}J^1_{\text{out}}\\ J^2_{\text{out}}\end{bmatrix}=s\begin{bmatrix}J^1_{\text{in}}\\ J^2_{\text{in}}\end{bmatrix}=\begin{bmatrix}r & t'\\ t & r'\end{bmatrix}\begin{bmatrix}J^1_{\text{in}}\\ J^2_{\text{in}}\end{bmatrix}\ , \tag{A18}$$

which can be written as

$$J^1_{\text{out}}=rJ^1_{\text{in}}+t'J^2_{\text{in}}\ , \tag{A19}$$

$$J^2_{\text{out}}=rJ^1_{\text{in}}+r'J^2_{\text{in}}\ . \tag{A20}$$

Compare Eqs. (A19) and (A20) with Eqs. (A16) and (A17); we obtain the overall reflection and transmission matrices cascaded from the reflection and transmission amplitudes of the individual scattering matrices of the two subsequent sections,

$$r=r_1+t'_1r_2(I_+-r'_1r_2)^{-1}t_1\ , \tag{A21}$$

$$t'=t'_1[r_2(I_+-r'_1r_2)^{-1}r'_1t'_2+t'_2]\ , \tag{A22}$$

$$t=t_2(I_+-r'_1r_2)^{-1}t_1\ , \tag{A23}$$

$$r'=t_2(I_+-r'_1r_2)^{-1}r'_1t'_2+r'_2\ . \tag{A24}$$

For a periodic structure consisting of N unit cells, the overall scattering matrix can be obtained from the scattering matrix for *one* unit cell by iteratively doing the above cascading process $N-1$ times,

$$s_N=s_{N-1}\otimes s_1=s_{N-2}\otimes s_1\otimes s_1=\ldots=s_1\otimes s_1\otimes\ldots\otimes s_1\ . \tag{A25}$$

To obtain correct results, it is necessary to include the evanescent states both in the outgoing and incoming states.

APPENDIX B: THE QUANTUM TRANSMITTING-BOUNDARY METHOD

In this appendix we provide a summary of the quantum transmitting-boundary method. Figure 12 illustrates the geometry of a two-dimensional quantum structure. It is partitioned into a "device" region Ω_0, and several lead regions $\Omega_1,\Omega_2,\ldots,\Omega_n$. The leads extend to infinity and in general are arbitrarily oriented. The boundary of the region Ω_0 is denoted Γ; the boundary between a lead region Ω_i and the device region Ω_0 is denoted Γ_i. The rest of the boundary Γ, which is not part of a lead boundary, is denoted Γ_0. A steady magnetic field $\vec{B}$ is applied in the perpendicular direction, that is $\vec{B}=B\hat{z}$. The main procedures of the QTBM algorithm are described in the following steps.

(1) Discretize the device region Ω_0 on a mesh, $\vec{r}_i=(x_i,y_i)$, $i=1,2,\ldots,M$. The potential $V(x,y)$ should be known at least on these nodal points.

(2) Choose a set of finite-element shape functions

$$\mathbf{N}(\vec{r})=\{\phi_i(\vec{r})\}=[\phi_1(\vec{r}),\phi_2(\vec{r}),\ldots,\phi_M(\vec{r})]\ , \tag{B1}$$

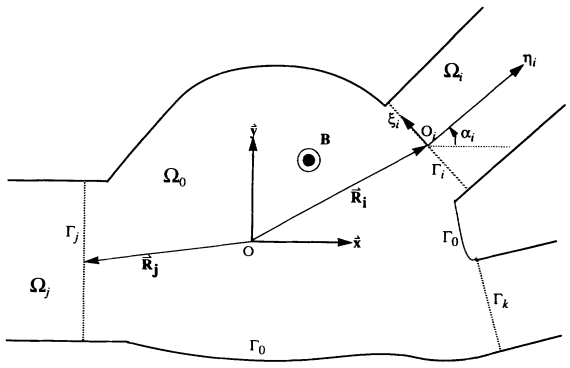

FIG. 12. A schematic diagram for a general two-dimensional device with multiple leads.

which obey

$$\phi_i(\vec{r}_j)=\delta_{ij} \ . \tag{B2}$$

Its first derivative matrix $\mathbf{B}(\vec{r})$ of dimension $(2\times M)$ is

$$\mathbf{B}(\vec{r})=\begin{bmatrix} \dfrac{\partial \mathbf{N}(\vec{r})}{\partial x} \\ \dfrac{\partial \mathbf{N}(\vec{r})}{\partial y} \end{bmatrix} = \begin{bmatrix} \dfrac{\partial \phi_1(\vec{r})}{\partial x} & \dfrac{\partial \phi_2(\vec{r})}{\partial x} & \cdots & \dfrac{\partial \phi_M(\vec{r})}{\partial x} \\ \dfrac{\partial \phi_1(\vec{r})}{\partial y} & \dfrac{\partial \phi_2(\vec{r})}{\partial y} & \cdots & \dfrac{\partial \phi_M(\vec{r})}{\partial y} \end{bmatrix} . \tag{B3}$$

(3) Construct the $M\times M$ matrices T, O, and V, using

$$\mathbf{T}\equiv\int_{\Omega_0}\frac{\hbar^2}{2m^*}\mathbf{B}^T(\vec{r})\mathbf{B}(\vec{r})d^2r \ , \tag{B4}$$

$$\mathbf{O}\equiv\int_{\Omega_0}\frac{i\hbar|e|B}{2m^*}\mathbf{N}^T(\vec{r})y\frac{\partial \mathbf{N}}{\partial x}d^2r \ , \tag{B5}$$

$$\mathbf{V}\equiv\int_{\Omega_0}\left[\frac{(|e|By)^2}{2m^*}+V_0(x,y)-E\right]\mathbf{N}^T(\vec{r})d^2r \ , \tag{B6}$$

where $V_0(x,y)$ is the potential energy in the device region Ω_0.

(4) For each lead i, construct a local coordinate system $O_i-\eta_i\xi_i$ with $\hat{\eta}_i$ pointing down the direction parallel to the lead walls and $\hat{\xi}_i$ pointing across the transverse direction across the lead. The potential energy $V_i(\xi_i)$ in the lead region can vary across the transverse coordinate ξ_i but is independent of the longitudinal coordinate η_i by the virtue of lead definition. Choose the Landau gauge in the local coordinate system as

$$\vec{A}'=-B\xi_i\hat{\eta}_i \tag{B7}$$

and the wave function in the lead region has the form

$$\Psi_i'=e^{ik^i\eta_i}\Upsilon^i(\xi_i) \ . \tag{B8}$$

Then solve the Schrödinger equation as an eigenvalue problem of the wave vector k^i for the transverse mode $\Upsilon^i(\xi_i)$ at incident energy E:

$$\left[-\frac{\partial^2}{\partial\xi_i^2}+\left[\frac{|e|B\xi_i}{\hbar}+k^i\right]^2+\frac{2m^*}{\hbar^2}V_i(\xi_i)\right]\Upsilon^i(\xi_i) =\frac{2m^*}{\hbar^2}E\Upsilon^i(\xi_i) \ . \tag{B9}$$

(5) Transfer the lead wave function Eq. (B8) for the locally defined gauge Eq. (B7) to the globally defined gauge

$$\vec{A}=-By\hat{x} \ , \tag{B10}$$

using

$$\Psi=e^{-ieG/\hbar}\Psi' \ , \tag{B11}$$

where G is the gauge transformation function defined by $\vec{A}-\vec{A}'=\nabla G$. It can be expressed in the local coordinates as

$$G_i(\eta_i,\xi_i)=B\left[\frac{\xi_i^2-\eta_i^2}{2}\sin\alpha^i\cos\alpha^i+\eta_i\xi_i\sin^2\alpha^i -\eta_iR_y^i\cos\alpha^i+\xi_iR_y^i\sin\alpha^i\right] . \tag{B12}$$

(6) Calculate the $N_{\text{in}}^i\times N_{\text{out}}^i$ overlap matrix Θ^i and the $N_{\text{out}}^i\times N_{\text{out}}^i$ overlap matrix Λ^i between the transverse modes

$$\Theta^i=\{\theta_{n,m}^i\}\equiv\left\{\int_{\Gamma_i}\chi_n^i\phi_m^{i*}d\xi_i\right\} , \qquad \Lambda^i=\{\Lambda_{m_1,m_2}^i\}\equiv\left\{\int_{\Gamma_i}\phi_{m_1}^i\phi_{m_2}^{i*}d\xi_i\right\} , \tag{B13}$$

where $\chi_n^i(\xi_i)$ are the incoming modes and $\phi_m^i(\xi_i)$ are the outgoing modes and they are both part of the solution of Eq. (B9). N_{in}^i is the number of incoming modes and N_{out}^i is the number of outgoing modes, both including traveling and evanescent states.

(7) Calculate matrices $\mathbf{M}_{\text{in}}^i(N_{\text{in}}^i\times L^i)$, $\mathbf{M}_{\text{out}}^i(N_{\text{out}}^i\times L^i)$, and $\mathbf{Q}_{\text{out}}^i(N_{\text{out}}^i\times L^i)$ using

$$\mathbf{M}_{\text{in}}^i(n,l)=\int_{\Gamma_i}\left[\left[k_n^i-\frac{e}{\hbar}\frac{\partial G^i}{\partial\eta_i}\bigg|_{\eta_i=0}\right]e^{-ieG_0^i/\hbar}\chi_n^i\right]\mathbf{N}_l^i d\Gamma_i \ , \tag{B14}$$

$$\mathbf{M}_{\text{out}}^i(m,l)=\int_{\Gamma_i}\left[\left[k_m^i-\frac{e}{\hbar}\frac{\partial G^i}{\partial\eta_i}\bigg|_{\eta_i=0}\right]e^{-ieG_0^i/\hbar}\varphi_m^i\right]\mathbf{N}_l^i d\Gamma_i \ , \tag{B15}$$

$$\mathbf{Q}_{\text{out}}^i(m,l)=\int_{\Gamma_i}(e^{-ieG_i^0/\hbar}\varphi_m^i)\mathbf{N}_l^i d\Gamma_i \ , \tag{B16}$$

where $G_0^i\equiv G^i(\eta_i,\xi_i)|_{\eta_i=0}$, $\mathbf{N}^i=(\mathbf{N}_1^i,\ldots,\mathbf{N}_l^i,\ldots,\mathbf{N}_{L^i}^i)$ are the global shape functions on the boundary Γ_i and L^i is the number of nodal points on the boundary.

(8) Calculate the boundary terms of matrix $\mathbf{C}_i$ and vector $\mathbf{P}_i$ from

$$\mathbf{C}_i\equiv-\frac{\hbar^2}{2m^*}(\Lambda^{i^{-1}}\mathbf{M}_{\text{out}}^i)^T(\mathbf{Q}_{\text{out}}^i)^* \ , \tag{B17}$$

$$P_i\equiv\frac{\hbar^2}{2m^*}(\vec{a}^i\mathbf{M}_{\text{in}}^i-\vec{a}^I\Theta^i\Lambda^{i^{-1}}\mathbf{M}_{\text{out}}^i)^T \ , \tag{B18}$$

where $\vec{a}^i=(a_1^i,a_2^i,\ldots,a_{N_{\text{in}}^i}^i)$ are the amplitudes of the incident wave function on the incoming modes. Then embed $\mathbf{C}_i$ and $\mathbf{P}_i$ for lead i into the $M\times M$ global matrix C and the $M\times 1$ array $\mathbf{P}$, done in the assembly process in the finite-element method.

(9) The discretized wave function then can be obtained by solving the following linear system for the unknown values $\mathbf{u}$ of the wave function at the nodal points

$$(\mathbf{T}+\mathbf{O}+\mathbf{V}+\mathbf{C})\mathbf{u}=\mathbf{P} \ . \tag{B19}$$

Once $\mathbf{u}$ is solved, other physical quantities of interest, for

example, current-density distribution can be obtained too.

(10) For obtaining the complex reflection and transmission matrices, Eq. (B19) is solved for multiple columns of right-hand side **P**, corresponding to injecting electrons at one mode one time with full amplitude. The $N^i_{\rm out}\times N^i_{\rm in}$ reflection matrix r^i in lead i and the $N^i_{\rm out}\times N^i_{\rm in}$ transmission matrix $t^{i\to j}$ from lead i to lead j can be computed from

$$r^i=-(\Theta^i\Lambda^{i^{-1}})^T+(\Lambda^{i^{-1}})^T Q^{i^*}_{\rm out}\mathbf{U}^i\,, \tag{B20}$$

$$t^{i\to j}=(\Lambda^{j^{-1}})^T Q^{j^*}_{\rm out}\mathbf{U}^j\,, \tag{B21}$$

where $\mathbf{U}^i=(\mathbf{u}^i_1,\mathbf{u}^i_2,\ldots,\mathbf{u}^i_{N^i_{\rm in}})$ and $\mathbf{U}^j=(\mathbf{u}^j_1,\mathbf{u}^j_2,\ldots,\mathbf{u}^j_{N^i_{\rm in}})$ are the wave functions on the lead boundaries Γ_i and Γ_j when the incoming wave at lead i is fully in the mode $1,2,..,N^i_{\rm in}$, respectively.

[1]D. A. Wharam, T. J. Thornton, R. Newbury, M. Pepper, H. Ahmed, J. E. F. Frost, D. G. Hasko, D. C. Peacock, D. A. Ritchie, and G. A. C. Jones, J. Phys. C **21**, L209 (1988).

[2]B. J. van Wees, H. van Houten, C. W. J. Beenakker, J. G. Williamson, L. P. Kouwenhoven, D. van der Marel, and C. T Foxon, Phys. Rev. Lett. **60**, 848 (1988).

[3]R. Landauer, IBM J. Res. Dev. **1**, 223 (1957); D. S. Fisher and L. A. Lee, Phys. Rev. B **23**, 6851 (1981).

[4]A. Weisshaar, J. Lary, S. M. Goodnick, and V. K. Tripathi, Proc. SPIE **1284**, 45 (1990); S. E Ulloa, E. Castaño, and G. Kirczenow, *ibid.* **1284**, 57 (1990); Hua Wu and D. W. Sprung, Phys. Rev. B **47**, 1500 (1993).

[5]Craig S. Lent, Srinivas Sivaprakasam, and D. J. Kirkner, Solid-State Electron. **32**, 1137 (1989); Craig S. Lent, Appl. Phys. Lett. **56**, 2554 (1990); **57**, 1678 (1990); Henry Harbury, Wolfgang Porod, and Craig S. Lent, Superlatt. Microstruct. **11**, 189 (1992).

[6]J. A. Nixon, J. H. Davies, and H. U. Baranger, Phys. Rev. B **43**, 12 638 (1991).

[7]Manhua Leng and Craig S. Lent, Phys. Rev. Lett. **71**, 137 (1993).

[8]See also the miniband transport in a channel with a modulated potential described by S. E. Ulloa, E. Castaño, and G. Kirczenow, Phys. Rev. B **41**, 12 350 (1990).

[9]B. J. van Wees, L. P. Kouwenhoven, H. Van Houten, C. W. Beenakker, J. E. Mooij, C. T. Foxon, and J. J. Harris, Phys. Rev. B **38**, 3625 (1988).

[10]*The Quantum Hall Effect,* edited by R. E. Prange and S. M. Girvin (Springer-Verlag, New York, 1990).

[11]S. Datta, *Quantum Phenomena* (Addison-Wesley, Reading, MA, 1989), p. 21.

[12]A. D. Stone and A. Szafer, IBM J. Res. Dev. **32**, 384 (1988).

[13]Craig S. Lent and D. J. Kirkner, J. Appl. Phys. **67**, 6353 (1990).

[14]Manhua Leng and Craig S. Lent, J. Appl. Phys. **76**, 2240 (1994).

[15]A. Szafer and A. D. Stone, Phys. Rev. Lett. **62**, 300 (1989); A. D. Stone and A. Szafer, in *Nanostructure Physics and Fabrication,* edited by M. A. Reed and W. P. Kirk (Academic, Boston, 1989), p. 369.

[16]G. Kirczenow, Solid State Commun. **68**, 715 (1988).

[17]E. Castaño and G. Kirczenow, Phys. Rev. B **45**, 1514 (1992).

[18]See discussions by G. Timp, R. Behringer, S. Sampere, J. E. Cunningham, and R. E. Howard, in *Nanostructure Physics and Fabrication* (Ref. 15), p. 311.

[19]A similar structure with 16 periods has been realized, see the article by L. P. Kouwenhoven, F. W. J. Hekking, B. J. von Wees, C. J. P. M. Harmans, C. E. Timmering, and C. T. Foxon, Phys. Rev. Lett. **65**, 316 (1990). In their experiments, Kouwenhoven *et al.* were not able to observe the miniband formation or quantized conductance plateaus in zero magnetic field, presumably due to impurity or potential fluctuations.

[20]The appearance of conductance zeros corresponding to the gaps in the band structure has been noted by others. See Ref. 4.

[21]Zhi-an Shao, Wolfgang Porod, and Craig S. Lent, Phys. Rev. B **49**, 7453 (1994).

[22]In an examination of the energy-band formation of a one-dimensional array of *T*-stub structures, we have found that as the quasibound states (transmission poles) of the system in the complex energy plane are nearing the real energy axis, the oscillations in the transmission on the real energy axis are more rapid. We have observed that oscillations are more prominent and persistent for some bands when the system is incommensurate [M. Leng and C. S. Lent (unpublished)].

[23]M. Büttiker, Phys. Rev. B **38**, 9375 (1988).

[24]L. P. Kouwenhoven, dissertation, Delft University of Technology, Delft, The Netherlands, 1992.

[25]For a full examination of the band structure of this structure in a magnetic field, see Craig S. Lent and Manhua Leng, Appl. Phys. Lett. **58**, 1650 (1991); J. Appl. Phys. **70**, 3157 (1991).

[26]See *Solid State Physics,* edited by Henry Ehrenreich and David Turnbull (Academic, San Diego, 1991), p. 175.

[27]K. von Klitzing, G. Dorda, and M. Pepper, Phys. Rev. Lett. **45**, 494 (1980).

[28]G. Müller, D. Weiss, A. V. Khaetskii, K. von Klitzing, S. Koch, H. Nickel, W. Schlapp, and R. Lösch, Phys. Rev. B **45**, 3932 (1992).

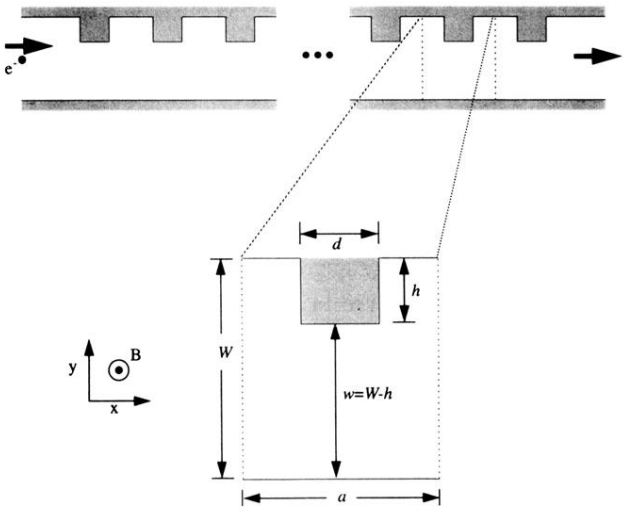

FIG. 1. The geometry of the periodically modulated quantum channel.

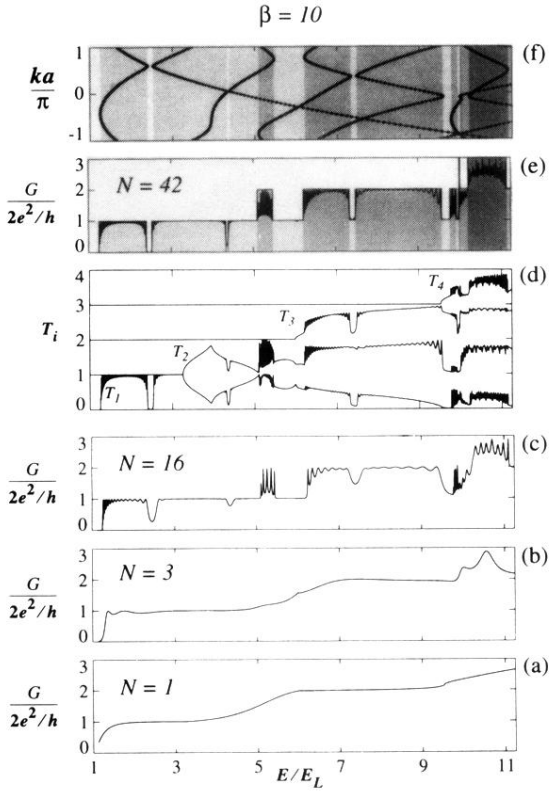

FIG. 10. The sinusoidally modulated channel in an applied magnetic field of $\beta=10$. (a) Conductance for a short channel with 1 unit cell ($N=1$): a QPC structure. (b) Conductance for a short channel with 2 unit cells ($N=3$). (c) Conductance for a channel with 16 unit cells ($N=16$). (d) Transmission coefficients of individual modes (edge states) for a long channel with 42 unit cells ($N=42$). (e) Conductance for the long channel with $N=42$ unit cells. Gray-scale shadings indicate the index of the quantization plateau. (f) The energy band structure for the infinite periodic channel. Gray-scale shadings indicate the number of individual energy bands with positive group velocity in each energy region. The correspondence of the shading schemes in (e) and (f) illustrates that the conductance of the finite channel is related to the number of positive-velocity bands in the band structure of the infinite channel.

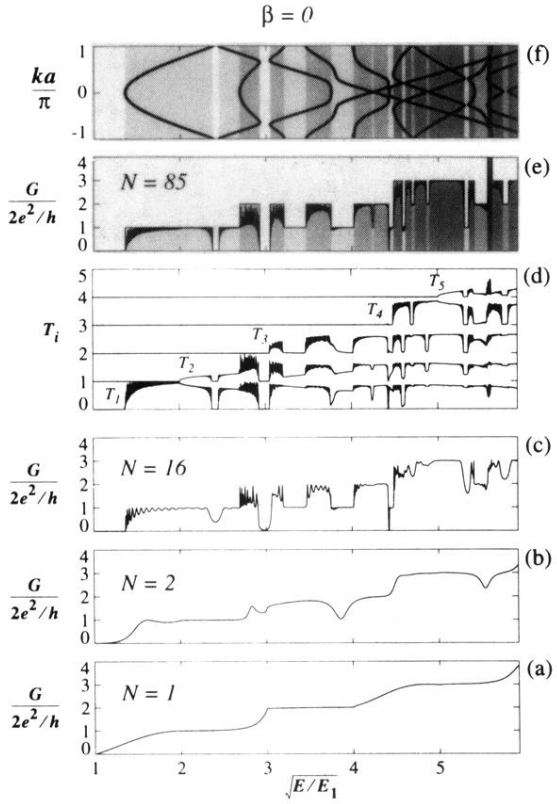

FIG. 2. The modulated channel in no applied magnetic field. (a) Conductance for a short channel with 1 unit cell ($N=1$): a QPC structure. (b) Conductance for a short channel with 2 unit cells ($N=2$). (c) Conductance for a channel with 16 unit cells ($N=16$). (d) Transmission coefficients of individual modes for a long channel with 85 unit cells ($N=85$). (e) Conductance for the long channel with $N=85$ unit cells. Gray-scale shadings indicate the index of the quantization plateau. (f) The energy band structure for the infinite periodic channel. Gray-scale shadings indicate the number of individual energy bands with positive group velocity in each energy region. The correspondence of the shading schemes in (e) and (f) illustrates that the conductance of the finite channel is related to the number of positive-velocity bands in the band structure of the infinite channel.

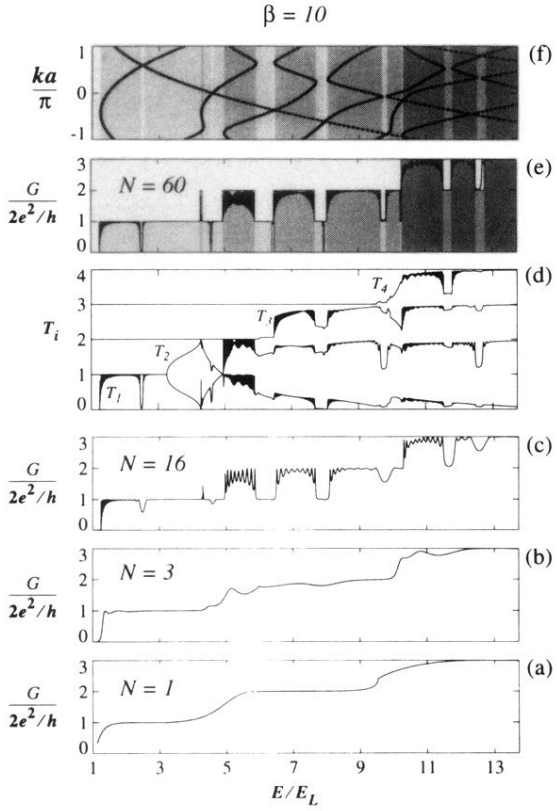

FIG. 3. The modulated channel in an applied magnetic field of $\beta=10$. (a) Conductance for a short channel with 1 unit cell ($N=1$): a QPC structure. (b) Conductance for a short channel with 2 unit cells ($N=3$). (c) Conductance for a channel with 16 unit cells ($N=16$). (d) Transmission coefficients of individual modes (edge states) for a long channel with 60 unit cells ($N=60$). (e) Conductance for the long channel with $N=60$ unit cells. Gray-scale shadings indicate the index of the quantization plateau. (f) The energy band structure for the infinite periodic channel. Gray-scale shadings indicate the number of individual energy bands with positive group velocity in each energy region. The correspondence of the shading schemes in (e) and (f) illustrates that the conductance of the finite channel is related to the number of positive-velocity bands in the band structure of the infinite channel.

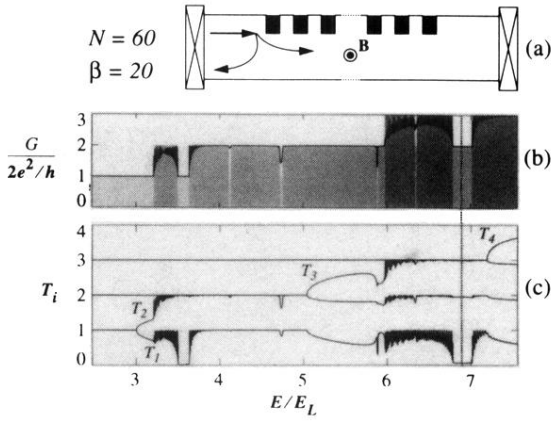

FIG. 4. (a) A modulated channel with straight leads connected to the source and drain. Incident electrons are in the subbands defined in the straight lead regions. (b) Conductance for such a channel with $N=60$ unit cells. (c) Transmission coefficients of individual modes (edge states).

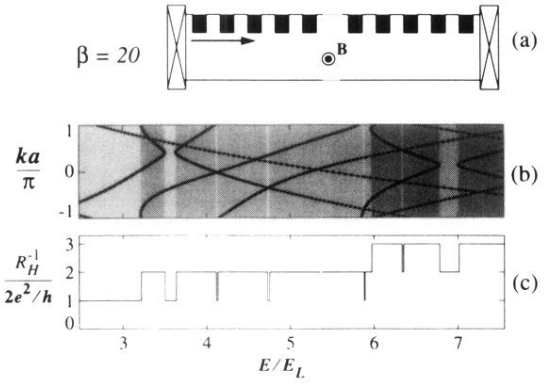

FIG. 6. (a) A very long modulated channel with modulations extended to the leads. Electrons are injected from the source onto the Bloch states. No backscattering occurs for such incident electrons. The two-terminal conductance is equivalent to the inverse of the Hall resistance. (b) The energy-band structure for the infinite periodic channel at $\beta=20$. (c) The inverse of the Hall resistance derived from the energy band structure.

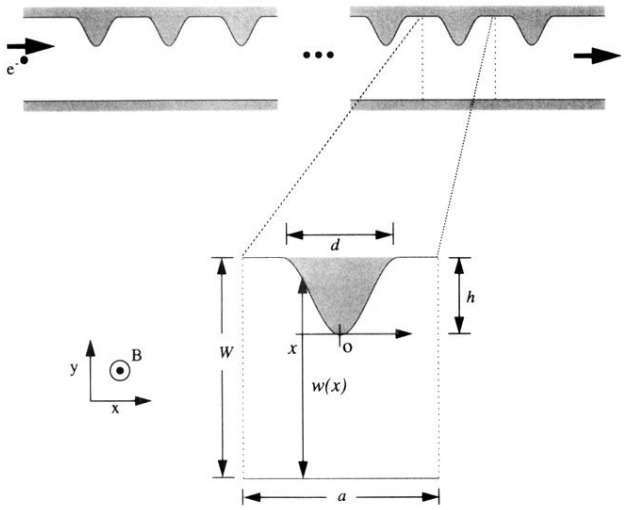

FIG. 8. The geometry of a periodically modulated quantum channel with sinusoidal modulations.

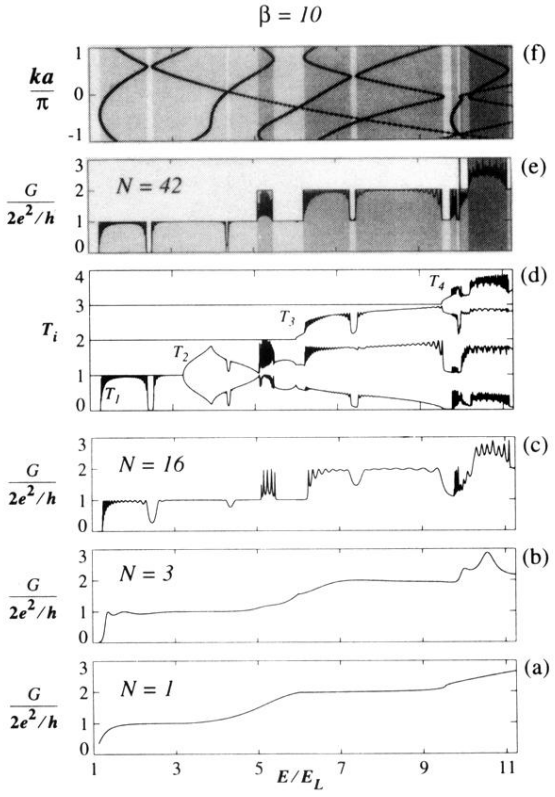

FIG. 10. The sinusoidally modulated channel in an applied magnetic field of $\beta=10$. (a) Conductance for a short channel with 1 unit cell ($N=1$): a QPC structure. (b) Conductance for a short channel with 2 unit cells ($N=3$). (c) Conductance for a channel with 16 unit cells ($N=16$). (d) Transmission coefficients of individual modes (edge states) for a long channel with 42 unit cells ($N=42$). (e) Conductance for the long channel with $N=42$ unit cells. Gray-scale shadings indicate the index of the quantization plateau. (f) The energy band structure for the infinite periodic channel. Gray-scale shadings indicate the number of individual energy bands with positive group velocity in each energy region. The correspondence of the shading schemes in (e) and (f) illustrates that the conductance of the finite channel is related to the number of positive-velocity bands in the band structure of the infinite channel.